Biol. Cybern. 87, 10–26 (2002)
DOI 10.1007/s00422-002-0311-8

Biological Cybernetics

Adaptation of reflexive feedback during arm posture to different environments

Erwin de Vlugt, Alfred C. Schouten, Frans C. T. van der Helm

Man-Machine Systems and Control, Department of Mechanical Engineering, Delft University of Technology, Mekelweg 2, 2628 CD Delft, The Netherlands

Received: 23 July 2001 / Accepted in revised form: 15 January 2002

Abstract. In this study we have examined the ability of the central nervous system (CNS) to use spinal reflexes to minimize displacements during postural control while continuous force perturbations were applied at the hand. The subjects were instructed to minimize the displacements of the hand from a reference position that resulted from the force perturbations. The perturbations were imposed in one direction by means of a hydraulic manipulator of which the virtual mass and damping were varied. Resistance to the perturbations came from intrinsic and reflexive stiffness, and from the virtual environment. It is hypothesized that reflexive feedback during posture maintenance is optimally adjusted such that position deviations are minimal for a given virtual environment. Frequency response functions were estimated, capturing all mechanical properties of the arm at the end point (hand) level. Intrinsic and reflexive parameters were quantified by fitting a linear neuromuscular model to the frequency responses. The reflexive length feedback gain increased strongly with damping and little with the eigenfrequency of the total combined system (i.e. arm plus environment). The reflexive velocity feedback gain decreased slightly with relative damping at the largest eigenfrequency and more markedly at smaller eigenfrequencies. In the case of highest reflex gains, the total system remained stable and sufficiently damped while the responses of only the arm were severely underdamped and sometimes even unstable. To further analyse these results, a model optimization was performed. Intrinsic and reflexive parameters were optimized such that two criterion functions were minimized. The first concerns performance and penalized hand displacements from a reference point. The second one weights afferent control effort to avoid inefficient feedback. The simulations showed good similarities with the estimated values. Length feedback was adequately predicted by the model for all conditions. The predicted velocity feedback gains were larger in all cases, probably indicating a mutual gain limiting relation between length and velocity afferent signals. The results suggest that both reflex gains seem to be adjusted by the CNS, where in particular the length feedback gain was optimal so as to maximize performance at minimum control effort.

Correspondence to: E. de Vlugt
(e-mail: e.devlugt@wbmt.tudelft.nl,
Tel.: +31-15-2785247, Fax: +31-15-2784717)

1 Introduction

Human posture control is basically characterized by minimization of position deviations from a reference position. In most cases, these deviations result from external force perturbations acting upon the body. Formalizing the body as a system excited by forces and reacting with corresponding movements, it is appropriately described as a mechanical admittance (dynamic relation between an input force and an output position). Low admittance (large stiffness and damping) results in high resistance to perturbations. Admittance reduction during posture maintenance can be realized by two mechanisms: (1) cocontraction and (2) afferent feedback. Cocontraction increases intrinsic muscle stiffness and damping at the expense of metabolic energy. Afferent length and velocity feedback from muscle spindles can further increase stiffness and damping. Since reflexive feedback introduces phase lags due to inherent neural time delays, its effectiveness is limited in avoiding oscillations.

The ability of the central nervous system (CNS) to specifically adjust length and velocity reflex gains to correct for displacements has been demonstrated in previous studies for the whole arm or segments of it (Bennett et al. 1993; Doemges and Rack 1992a,b; Dufresne et al. 1978; Hogan 1985; Lacquaniti and Soechting 1986).

Adjusting the reflex gains changes the arm admittance at relatively small metabolic energy cost because muscles are only activated when stretched. Therefore it is hypothesized that under conditions where force

perturbations are present or expected, reflex gains are modulated such that the arm admittance is decreased and the resulting position deviations are minimized.

In Van der Helm (submitted, 2002) the human arm was disturbed with stochastic force perturbations having different frequency content. For small-bandwidth perturbations that did not excite the eigenfrequency of the arm (±3 Hz), the reflex gains were substantial. With increasing bandwidth of the perturbation the gains decreased to avoid oscillations around the eigenfrequency. This is because oscillations worsen performance. In nearly all cases, the estimated gains led to boundary stable solutions of the model indicating that performance was always close to optimal.

A model study by De Vlugt et al. (2001) demonstrated that the experimental feedback gains were nearly optimal. Schouten et al. (2001) used a two degree-of-freedom musculoskeletal model with six muscles – including non-linear actuator and sensor dynamics – to simulate the experiments. It was demonstrated that under these particular experimental conditions (small position deviations), linearization of the neuromuscular system was appropriate. Again, reflex gains were found to be substantial and directly determined by the task requirements and stability constraint, indicating that control-effort weighting played a minor role under the experimental conditions.

When the arm is physically attached to an environment (i.e. a manipulator) the total combined admittance is the parallel connection of arm admittance $H_{\mathrm{arm}}(s)$ and admittance of the environment $H_{\mathrm{e}}(s)$ (called the environmental admittance); see Fig. 1. All system descriptions will be expressed in the frequency domain with $s = \lambda + j2\pi f$ ($\lambda = 0$ because the initial transient response is not of interest). The relation between force and position is:

$$D(s) = \left[H_{\mathrm{arm}}^{-1}(s) + H_{\mathrm{e}}^{-1}(s)\right]X(s) \tag{1}$$

where $D(s)$ is the force disturbance and $X(s)$ is the common position of hand and environment, such that the combined admittance $H_{DX}(s)$ with force as the input (causal form) becomes:

$$H_{DX}(s) = \frac{X(s)}{D(s)} = \frac{H_{\mathrm{arm}}(s)H_{\mathrm{e}}(s)}{H_{\mathrm{arm}}(s) + H_{\mathrm{e}}(s)} \tag{2}$$

The performance and stability are now determined by the mechanical properties of the combined system. Changing the properties of the environment evidently changes the effect of the arm admittance on the combined (total) behaviour. The combined admittance is dominated by the system having the lowest admittance (Eq. 2). Milner and Cloutier (1993) demonstrated the influence of an unstable environment on reflex feedback from wrist muscles. They attached the wrist to a manipulator, the damping of which was negatively increased and caused the relative damping of the combined system to decrease. It was demonstrated that reflexive feedback was reduced when external damping became more negative. These reflex gain adjustments are in accordance with the role of the CNS as being an optimal controller: decreasing the relative damping of the combined system reduces the stability margins such that reflexive feedback must be tempered to prevent oscillations.

In the aforementioned studies, stability was always a constraint to the adjustments of reflexes. When the admittance of the environment decreases, thereby increasing the stability margins, the question arises whether the CNS makes use of these favourable conditions. More specifically, does an increase in damping of the environment result in higher reflexive feedback? And, if so, is there still a constraint (when stability is not one anymore) such as a control-effort weighting to reflex gain adjustment for these conditions?

The goal of this study is to demonstrate the modulation of reflexes of the arm when external admittance decreases. For this purpose, experiments were performed using a number of relative damping ratios and eigenfrequencies of the combined system in order to investigate the effect on reflex gains. The experimental results are compared with optimizations of a lumped linear model including control-effort weighting.

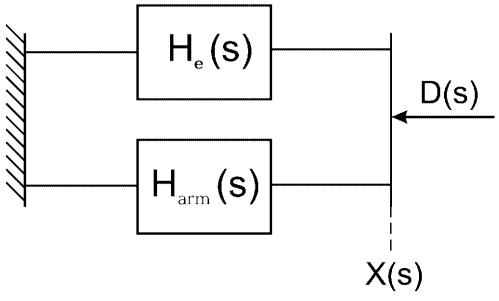

Fig. 1. Schematic configuration of parallel coupling of arm admittance $H_{\mathrm{arm}}(s)$ and environmental admittance $H_{\mathrm{e}}(s)$ (m/N). The combined admittance is the dynamic relation between the force disturbance $D(s)$ and end point (common position of hand and environment) $X(s)$, where $X(s)$ represents the displacements between the end point and the fixed world

2 Materials and methods

2.1 Subjects

Five normal healthy subjects (three men, two women, age range 20–26 years) participated voluntarily in this study. They had no history of musculoskeletal or neurological disease. The experiments were carried out with the right arm. All the subjects gave their informed consent to the experimental procedure.

2.2 Apparatus

A linear, hydraulically driven manipulator was used to generate force perturbations on the hand in horizontal directions. A load cell is mounted between the handle

and the piston of the manipulator to measure the hand force applied by the subject to the manipulator. This force is electronically translated into a movement corresponding to a (virtual) environmental admittance consisting of a linear second-order mass-damper-spring combination. Its values can vary in the range 0.6–20 kg for the mass m_e, 0.6–400 Ns/m for the damping b_e and 0.1–250 N/m for the stiffness k_e. The position of the hand results from the force input and the environmental admittance. This position is imposed on the subject by the position control loop of the manipulator. Force perturbations are imposed by adding an external input signal to the measured hand force.

2.3 Force perturbation

The force perturbation was the same throughout all the experiments, containing frequencies in the range 0.05–20 Hz. The perturbation signal was generated off-line in the frequency domain, such that within the bandwidth the power has a constant value, whereas the phase is chosen as a random value with a uniform distribution between 0 rad and 2π rad. The result is transformed to the time domain by inverse Fourier transformation. The duration of each perturbation was limited to 40 s, a sufficient observation time without causing significant fatigue. Figure 2 shows a 5-s sample of the time course of the force perturbation together with its power spectrum. As a result of the random distribution of the phases, the signal was stochastic and unpredictable for the subjects. The signal was passed through a digital-to-analogue (D/A) converter with a reconstruction frequency of 125 Hz and applied as input to the manipulator. By adjusting the power of the force perturbation, the hand displacements were kept sufficiently small ($\pm$1 cm in amplitude in all cases) to justify the linear-model approximation.

2.4 Recording

The following signals were measured via A/D conversion with 12-bit resolution at a 500 Hz sample frequency and digitally stored: hand position $x_h(t)$, interaction force $f_h(t)$, external force perturbation $d(t)$ and four EMG signals. EMG was measured using differential electrodes, pre-amplified, high-pass filtered (20 Hz, third-order Butterworth), amplified, rectified and smoothed at 200 Hz (low-pass, third-order Butterworth).

Surface EMG was used to validate the estimated co-contraction level. Activation of four relevant muscles around the shoulder were measured: for the anteflexors, pectoralis major (pars clavicularis) and deltoideus anterior; and for the retroflexors, deltoideus posterior and latissimus dorsi.

Since only stationary behaviour was of interest, initial transient effects were eliminated by rejecting the first 3616 samples ($\approx$7 s) from each time record, leaving 16 384 ($= 2^{14}$) samples for further analysis.

2.5 Experimental procedures

The subject was seated in a chair (Fig. 3) and asked to take a firm grip on the handle in order to minimize movements of the handle with respect to the hand. The motion of the hand was constrained by the manipulator to move only in the anterior–posterior direction (shoulder and elbow rotations were dependent). The forearm was horizontally

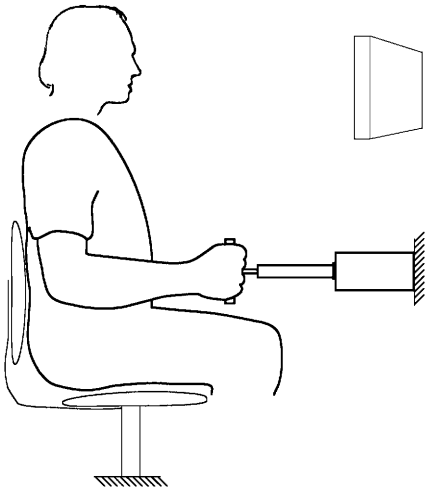

Fig. 3. Experimental setup showing the subject sitting upright on a chair with back support, holding the handle mounted on the piston of a hydraulic actuator. The interaction force generated by the subject on to the handle was measured by a force transducer located between the handle and the piston. The actual and reference handle positions were displayed on a monitor in front of the subject

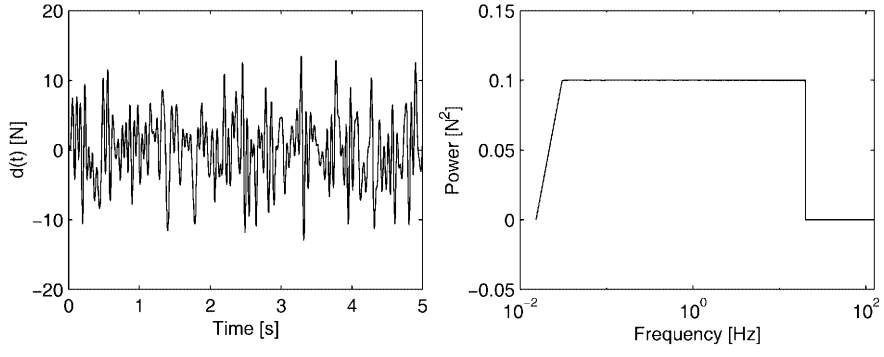

Fig. 2. *Left*: 5-s sample of the force perturbation $d(t)$. *Right*: power spectrum of $d(t)$

aligned with the piston and the elbow was flexed 90° such that the upper arm was vertically aligned. This is referred to as the reference position. In order to minimize movement of the shoulder rotation center, the subjects were asked not to move their trunk. The task given to the subjects was to 'minimize displacements' resulting from the applied force perturbation. To prevent drifting, the actual hand position was presented to the subject on a display together with the reference position. The subjects were also motivated by the display, since increased effort resulted in visibly smaller displacements.

Afferent feedback from muscle spindle activity was most likely to be inhibited when wide-bandwidth (0.05–20 Hz) force perturbations were applied in the case of a high admittant environment, with $m_e = 0.6$ kg, $b_e = 0.6$ Ns/m and $k_e = 0.1$ N/m (F.C.T. Van der Helm, submitted, 2002). This result can be explained from the optimal control perspective: high feedback gains result in severe underdamped responses that would damage performance. This experimental procedure is repeated in this study to determine the intrinsic properties of the subject's arm (lumped end-point mass, damping and stiffness) by fitting an intrinsic model to the estimated arm admittance (Sect. 2.7) using a straightforward least-squares method in the frequency domain.

Based on the intrinsic properties of the arm, the damping of the environment (manipulator) was adjusted such that the relative damping, β, of the combined intrinsic system, (i.e. intrinsic arm plus environment) was assigned fixed values of 0.7 (critical), 1.0, 1.3, 1.6, and 1.9 (all overdamped).

Furthermore, three different values for the external mass m_e were taken: 0.6 kg, 5 kg and 10 kg. These values were the same for all subjects. The external stiffness was not changed and remained always at a minimum ($k_e = 0.1$ N/m). The eigenfrequency of the combined (intrinsic) system, f_{0_i}, then follows from the combined mass and stiffness.

For each eigenfrequency all values for relative damping were applied, resulting in fifteen different environmental mass–damping (MB) combinations. Three additional conditions were employed for each eigenfrequency in combination with minimal external damping ($b_e = 0.6$ Ns/m). These conditions represent the lowest attainable relative damping possible with the present equipment and will elicit human control behaviour under highly underdamped conditions. For each subject, this makes a total of eighteen MB combinations of relative damping and eigenfrequency applied. The order in which the combinations were applied to the subjects was randomly distributed to avoid any anticipation. Each condition was repeated four times to improve the estimates by time averaging, resulting in a total of 72 trials. Subjects were free to rest as long as they liked between trials. The complete experiment lasted approximately 3 hours for each subject.

For each MB combination, reflexive length and velocity feedback gains were estimated according to a procedure comparable to that used to obtain the intrinsic parameters. For this purpose, the intrinsic model was extended with a length and velocity reflex loop. Together with the reflexive parameters, intrinsic stiffness and damping were estimated by means of one value representing the amount of cocontraction that scales the intrinsic stiffness and damping values estimated under the highest admittance condition (see also Appendix A.1).

2.6 Spectral analyses

The combined system is perturbed by the independent external force perturbation signal $d(t)$. The measured hand reaction force $f_h(t)$ and hand position $x_h(t)$ are dependent signals inside the closed loop. The admittance of arm and combined system were non-parametrically estimated in the frequency domain, expressed as frequency response functions (FRFs). The estimator for the admittance of the combined system is

$$\hat{H}_{DX}(f) = \frac{\hat{S}_{dx}(f)}{\hat{S}_{dd}(f)} \tag{3}$$

where $\hat{H}_{DX}(f)$ is the estimated admittance of the combined system (arm plus environment); $\hat{S}_{dx}(f)$ is the estimated cross spectral density between force perturbation, $d(t)$, and hand displacement, $x_h(t)$; and $\hat{S}_{dd}(f)$ the estimated auto spectral density of $d(t)$. The spectral densities were obtained using the fast Fourier transformation of the corresponding time signals (Van Lunteren 1979).

To verify the validity of linear models, the coherence function is estimated. This function is a measure for the amount of linearity of the system in response to the external force perturbation and is determined according to

$$\hat{\Gamma}_{DX}(f) = \sqrt{\frac{|\hat{S}_{dx}(f)|^2}{\hat{S}_{dd}(f)\hat{S}_{xx}(f)}} \tag{4}$$

The coherence function $\hat{\Gamma}_{dx}(f)$ equals one when there is no noise (linearization or measurement noise), and zero in the worst case.

As the human controller is embedded in a closed-loop configuration, the estimate for the arm admittance was obtained using the closed-loop estimator:

$$\hat{H}_{\mathrm{arm}}(f) = \frac{\hat{S}_{dx}(f)}{\hat{S}_{df}(f)} \tag{5}$$

where $\hat{H}_{\mathrm{arm}}(f)$ is the estimated arm admittance and $\hat{S}_{df}(f)$ is the estimated cross-spectral density between the external force perturbation, $d(t)$, and reaction force $f_h(t)$. In all estimators – (3), (4) and (5) – the estimated of the auto- and cross-spectral densities were averaged over eight frequency points to reduce the variance (Jenkins and Watts 1969).

2.7 Parametric model

The intrinsic model includes arm and hand dynamics. The derivation of the intrinsic model is given in Appendix A.1. The intrinsic parameters to be estimated

are: arm mass, m_a; arm damping, b_a; arm stiffness, k_a; hand grip viscosity, b_h; and elasticity, k_h. Including the hand dynamics significantly improved the estimation of the intrinsic arm parameters, especially arm mass; this is because hand stiffness and viscosity values appeared to be much larger than those of the arm (Sect. 3), so that hand dynamics are present in the frequency range (about 10 Hz) where also the arm mass is dominant. In the following, when referring to the arm dynamics, the combined arm and hand dynamics are meant.

From the estimated intrinsic values, the MB combinations for each subject were determined as described in Sect. 2.5. Only for this purpose, hand dynamics were neglected such that the combined system can be described as a second-order system that facilitates the calculation of relative damping and eigenfrequencies.

The second-order dynamics of the intrinsic combined admittance $H_{DX_i}(s)$ follow from (2):

$$H_{DX_i}(s) = \frac{H_{arm}(s)H_e(s)}{H_{arm}(s) + H_e(s)} = \frac{1}{H_{arm}^{-1}(s) + H_e^{-1}(s)}$$

With

$$H_{arm}(s) = \frac{1}{m_a s^2 + b_a s + k_a}$$

$$H_e(s) = \frac{1}{m_e s^2 + b_e s + k_e}$$

the combined intrinsic system becomes

$$H_{DX_i}(s) = \frac{1}{(m_a + m_e)s^2 + (b_a + b_e)s + (k_a + k_e)} = \frac{1/k_{tot}}{\frac{1}{\omega_0^2}s^2 + \frac{2\beta}{\omega_0}s + 1} \quad (6)$$

where $m_{tot} = m_a + m_e$, $b_{tot} = b_a + b_e$ and $k_{tot} = k_a + k_e$; and with the eigenfrequency, f_{0_i}, and β the relative damping according to

$$f_{0_i} = \frac{1}{2\pi}\sqrt{\frac{k_{tot}}{m_{tot}}} \quad (7)$$

$$\beta = \frac{b_{tot}}{2\sqrt{k_{tot}m_{tot}}} \quad (8)$$

Substituting b_{tot} in (8) and rewriting it gives

$$b_e = 2\beta\sqrt{k_{tot}m_{tot}} - b_a \quad (9)$$

Using the controlled values for β and the external mass m_e, the external damping b_e follows from (9).

To estimate the reflex gains and the amount of cocontraction, the intrinsic model was extended with a reflex loop consisting of three elements: (1) reflexive length and velocity feedback gains, (2) third-order Pade approximation of neural transportation delay, and (3) first-order activation dynamics (see Appendix A.2). The parameters to be estimated were: reflexive length feedback gain, $\hat{k}_p$, reflexive velocity feedback gain, $\hat{k}_v$, and cocontraction level $\hat{u}_0$ (where the hat denotes the values derived from the estimated FRFs).

For each set of estimated parameters $\{\hat{k}_p, \hat{k}_v, \hat{u}_0\}$ the variance accounted for (VAF) was calculated indicating the 'goodness of fit' of the estimated combined model (arm plus environment) to the recorded values:

$$VAF = \left[1 - \frac{\sum_{i=1}^{n} |x_h(t_i) - x_{h,sim}(t_i)|^2}{\sum_{i=1}^{n} |x_h(t_i)|^2}\right] \cdot 100\% \quad (10)$$

where $x_{h,sim}(t_i)$ the forward simulated hand position and $x_h(t_i)$ is the measured hand position, where i indexes the time. The hand position, $x_{h,sim}(t_i)$, is obtained by simulations using the model of the combined system, $H_{DX}(s)$ (Appendix A.3, Eq. A9), including the estimated parameter values and the input force disturbance $d(t)$ identical to those used in the experiments.

For each MB combination, the recorded smooth EMG signals were averaged over four trials. Then, the root mean square (RMS) values were calculated. To compare variations between EMG (in millivolts) and the corresponding estimated cocontraction, $\hat{u}_0$, the RMS values were scaled. This scaling was such that the mean of the RMS values (for each muscle over all MB combinations and for each subject) equals the corresponding mean value of the estimates. The goodness of the estimate was represented as the difference between the scaled RMS and $\hat{u}_0$.

2.8 Model optimization

A model optimization was performed to assess the effect on the adjustments of reflexive feedback of: (1) the task variable (in this case this is the instruction to 'minimize displacements'), (2) the mechanical properties of the environment, and (3) the force perturbation. The task instruction was replaced by a performance criterion that weights displacements of the hand from the reference point. Another criterion was implemented to minimize control effort. The goal of the optimization is to minimize the combined criterion functions. The parameters to be optimized were the reflexive length and velocity feedback gains, k_p^* and k_v^*, respectively (asterisks denote optimized values).

The performance criterion is formulated as

$$J_x = E\{x_h^2(t)\} \quad (11)$$

where $E\{\cdot\}$ is the expectation operator. Because the model is expressed in the frequency domain, J_x is rewritten into its corresponding frequency form (see Appendix A.4 for the derivation):

$$J_x = \int_{f_l}^{f_h} |H_{DX}(f)|^2 df \quad (12)$$

where $H_{DX}(f)$ is the closed-loop transfer function of the combined system. J_x therefore depends on the gain of the closed-loop dynamics inside the input frequency range $f_l \le f \le f_h$. The mean estimated intrinsic values of all subjects were averaged for each MB combination and used in $H_{DX}(s)$ (see Table 1). Control-effort weighting

was added by a criterion function J_a and similar to the performance criterion is written in its frequency form:

$$J_a = E\{a^2(t)\} = \int_{f_l}^{f_h} |H_{DA}(f)^2| \mathrm{d}f \quad (13)$$

where $H_{DA}(s)$ is the closed-loop transfer function from force perturbation $d(t)$ to reflexive activation $a(t)$ (Appendix A.3, Eq. A11).

From (12) and (13) it is clear that the optimal closed-loop behaviour is determined by the frequency range of the input perturbation. Due to the performance criterion J_x, the reflex gains tend to increase – i.e. reducing the admittance $H_{DX}(f)$ – while the control-effort criterion $J_a(f)$ tends to limit the gains.

The parameters of the postural control model will be optimized by minimizing the summed cost function:

$$J = J_x + pJ_a \quad (14)$$

In addition to this cost function, the poles of the combined system $H_{DX}(s)$ were constrained to be in the left half of the complex plane to ensure stability.

Evidently, increasing the weighting factor p worsens performance and reduces control effort. One value for p was chosen for all conditions such that the optimized reflex gains were comparable in a qualitative way to the estimated ones (see Sect. 3).

The optimization is performed in the frequency domain, where (12) and (13) were numerically integrated between f_l and f_h at each optimization step.

The optimization is also used to calculate the sensitivity of the estimated feedback gains to the differences between measured EMG (scaled RMS) and estimated cocontraction levels. Therefore, the model was optimized using the estimated $\hat{\boldsymbol{u}}_0$ plus and minus the standard deviation of these differences.

The optimization uses a multidimensional constrained non-linear minimization method. All calculations for estimation and optimization are performed using MATLAB (The MathWorks, Noctick, Mass.).

An overview of the experimental and optimization procedures performed is shown in Fig. 4 in the form of a flow chart.

3 Results

3.1 Experiments

The MB combinations derived from the intrinsic values for subject H.B. are plotted in Fig. 5 as an example. Every open circle in this figure represents a single condition applied. The mutually shifted square root curves indicate lines of constant relative damping (β) according to (9). Vertical shifted points indicate conditions with the same eigenfrequency (f_{0_i}), i.e. where the mass of the environment is the same. The additional three conditions are shown on the horizontal axis, indicating the lowest relative damping applied being 0.50, 0.32 and 0.24 for this subject.

Figure 6 shows the estimated gain and phase of $H_{\mathrm{arm}}(f)$ of four extreme conditions for subject H.B., corresponding to the conditions indicated with large circles in Fig. 5. The corresponding admittances of the combined system $H_{DX}(f)$ are given in Fig. 7. Comparable responses were found for all other subjects.

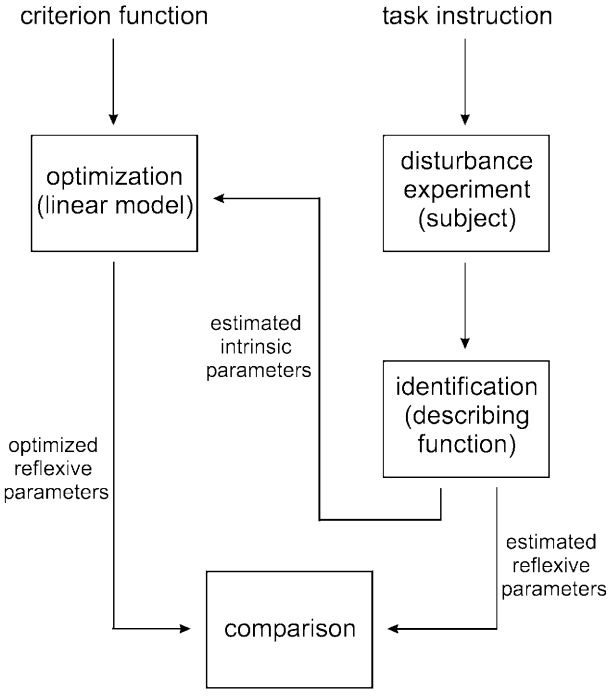

Fig. 4. Flowchart of the procedure followed in this study. The *right path* is the experimental execution with the subject taken as an optimal controller to minimize hand displacements. Its input–output behaviour (admittance) is estimated as a describing function from which lumped intrinsic and reflexive parameters were obtained by model fitting, as described in the text. The *left path* represents the optimization of the combined arm–environment model so as to simulate the experimental procedure where the criterion function mimics the task instruction given to the subject. Optimized reflex parameters were compared with the estimated ones

Table 1. Estimated intrinsic arm parameters and eigenfrequencies of all subjects ($n = 5$) and their standard deviation (SD)

	Mean (SD)	Unit	Description
m_a	1.88 (0.290)	kg	arm mass
b_a	37.3 (6.30)	Ns/m	intrinsic arm damping
k_a	733 (175)	N/m	intrinsic arm stiffness
b_h	178 (45.5)	Ns/m	intrinsic hand damping
k_h	14998 (50.5)	N/m	intrinsic hand stiffness
f_{0_i}	2.77 (0.191)	Hz	eigenfrequency of the combined intrinsic system
	1.69 (0.157)		
	1.31 (0.129)		

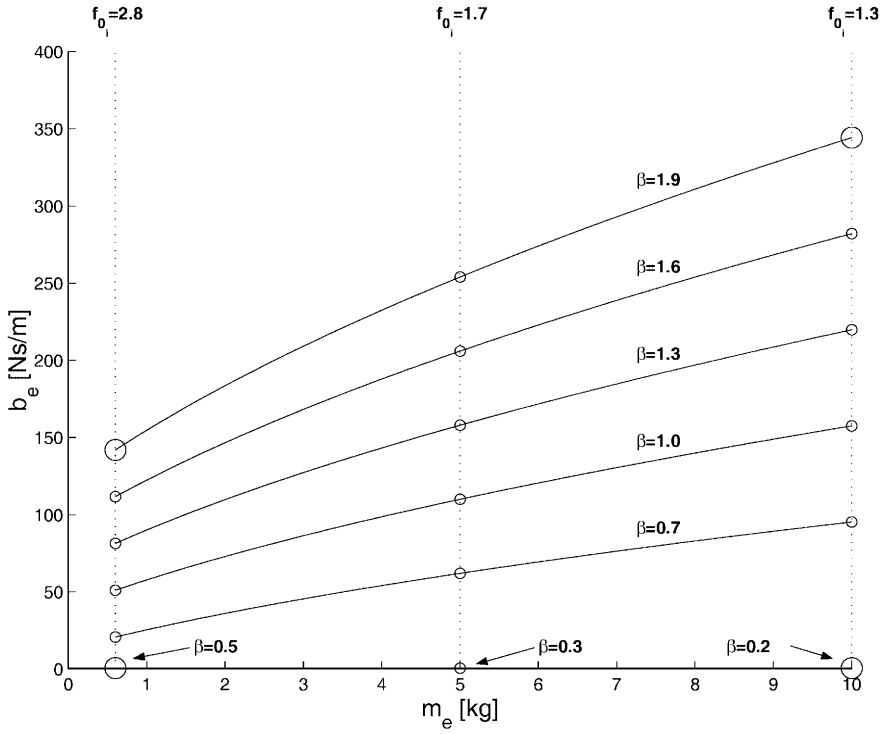

Fig. 5. Mass–damping (MB) combinations of parameters of the environment admittance based on intrinsic properties of subject H.B., represented by *open circles*. Each combination is an applied experimental condition. Square-root (interpolated) *curves* connect conditions with constant relative damping β (controlled variable) of the combined intrinsic system. Combinations on *vertical lines* have equal eigenfrequencies f_{0_i} (controlled variable) of the combined intrinsic system. *Circles* on the horizontal axis denote the three conditions with the lowest external damping, $b_e = 0.6$ Ns/m. *Large circles* denote four extreme conditions (see text). The large circle at the left on the horizontal axis denotes the condition where no reflexes were present, i.e. where the intrinsic parameters were determined

For all conditions, the estimated mean reflex gains amongst all subjects (mean and standard deviation) are given in Fig. 8 where the four conditions are indicated by vertical arrows.

The left plot of Fig. 6 (dashed curves) shows $H_{\mathrm{arm}}(s)$ in the case of the largest environmental admittance $H_e(s)$. From this condition the intrinsic parameters were estimated because no reflexes were likely to be present, as can be seen from Fig. 8 (leftmost arrow). Table 1 gives the average estimated intrinsic values among all subjects. The mean eigenfrequencies (Eq. 7) were $f_{0_i} = \{2.8, 1.7, 1.3\}$ Hz (see Table 1).

For the highest eigenfrequency, $f_{0_i} = 2.8$ Hz ($m_e = 0.6$ kg), the arm admittance showed a significant oscillation peak when relative damping is largest ($\beta = 1.9$; Fig. 6, left column, solid curves). This can be explained by an increased length feedback gain of approximately 500 N/m, which is about 75% of the intrinsic stiffness. Decreasing the eigenfrequency f_{0_i} to 1.3 Hz ($m_e = 10$ kg) results in an even more underdamped response of the arm admittance. In the case of the smallest relative damping ($\beta = 0.24$), there is already significant amplification at the eigenfrequency that still further increases to extremely underdamped behaviour for the largest relative damping ($\beta = 1.9$; Fig. 6, right column, solid curves). At these combinations of small eigenfrequencies and large values for relative damping, the arm sometimes became unstable. Note that arm instability never led to unstable behaviour of the combined system $H_{DX}(f)$. The length feedback gains (Fig. 8, arrows in third column) were high and exceeded the intrinsic stiffness by a factor of approximately 1.5. Generally, $\hat{k}_p$ increases with relative damping and its characteristics are shifted to larger values with increasing eigenfrequency f_{0_i}.

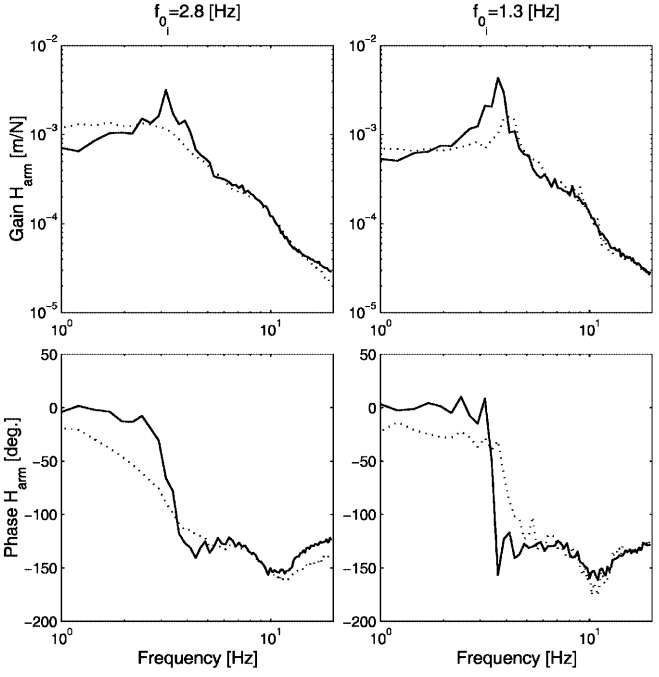

Fig. 6. Estimated transfer functions of the arm, $\hat{H}_{\mathrm{arm}}(f)$, for subject H.B. (averages of four trials). *Top row*: gain (m/N); *bottom row*: phase (degrees). *Left column*: largest eigenfrequency $f_{0_i} = 2.8$ Hz ($m_e = 0.6$ kg) and two different values for relative damping: $\beta = 0.5$ (*dashed curves*), at which the intrinsic parameters were measured, and $\beta = 1.9$ (*solid curves*) of combined intrinsic system; *right column*: $f_{0_i} = 1.3$ Hz ($m_e = 10$ kg) with $\beta = 0.24$ (*dashed curves*) and $\beta = 1.9$ (*solid curves*)

The velocity feedback gain $\hat{k}_v$ showed opposite variations, decreasing moderately with relative damping at all eigenfrequencies. Typically, the estimates became negative with increasing relative damping.

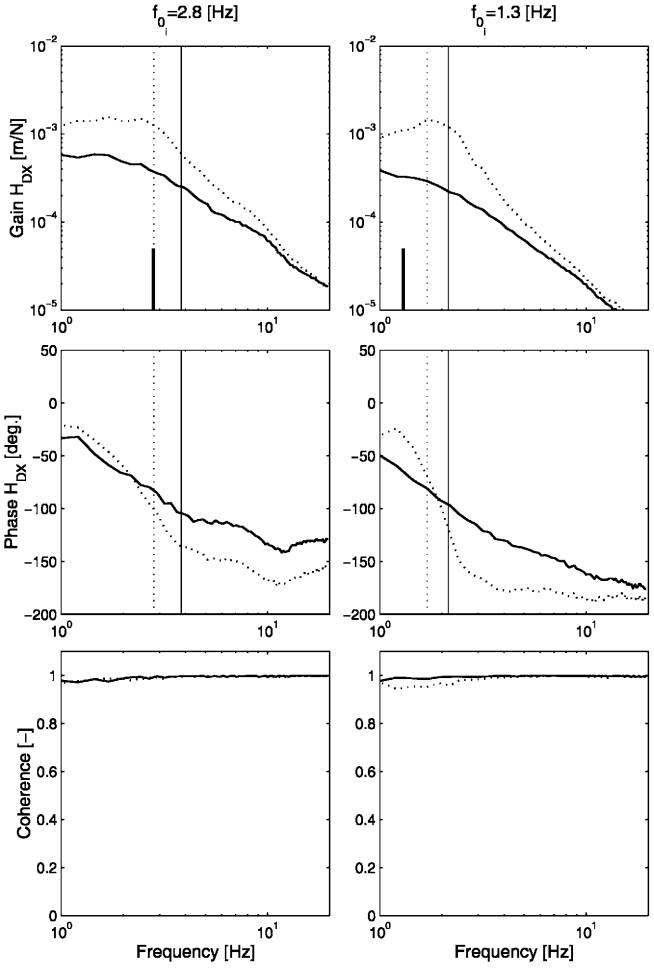

Fig. 7. Estimated transfer functions of combined system (arm plus environment) $\hat{H}_{DX}(f)$ for subject H.B. (averages of four trials). *Top row*: gain (m/N); *middle row*: phase (degrees); *bottom row*: coherence function $\hat{\Gamma}_{DX}(f)$. *Left column*: largest eigenfrequency $f_{0_i} = 2.8$ Hz ($m_e = 0.6$ kg) and two different values for relative damping: $\beta = 0.5$ (*dashed curves*) and $\beta = 1.9$ (*solid curves*) of the combined intrinsic system; *right column*: $f_{0_i} = 1.3$ Hz ($m_e = 10$ kg) with $\beta = 0.24$ (*dashed curves*) and $\beta = 1.9$ (*solid curves*). *Short vertical bars* on the horizontal axis indicate the eigenfrequencies (f_{0_i}) of the combined intrinsic system without reflexes. *Vertical lines* indicate the corresponding eigenfrequencies as the result of increased stiffness due to reflexes

In contrast to the arm admittance, the combined system was almost critically damped for the lowest values of β and severely overdamped for the highest values (Fig. 7). Comparison with the arm admittance, $H_{\mathrm{arm}}(f)$, immediately reveals that the low frequency gain of $H_{DX}(f)$ is determined by $H_{\mathrm{arm}}(f)$, and that the undesired oscillation peak of $H_{\mathrm{arm}}(f)$ is suppressed by the environment. For the largest values of β the arm compliance showed the highest oscillation peak, whereas the combined system was severely overdamped by the environment.

Since reflexive length feedback increases the stiffness of the arm and consequently that of the combined system, the eigenfrequencies based on the MB combinations shift to higher frequencies. This is indicated in Fig. 7 by vertical lines and by short vertical bars on the horizontal axis at f_{0_i}. The largest increase in eigenfrequency occurs at the largest values for β where $\hat{k}_p$ is largest (right arrows in first and third column of Fig. 8). For these conditions, the eigenfrequencies were shifted from 2.8 Hz to 3.8 Hz and from 1.3 Hz to 2.1 Hz, respectively.

In nearly all cases the estimated coherence $\hat{\Gamma}_{DX}(f)$ was high (> 0.9) for all frequencies, which validates the linear model approximation and proves that measurement noise was negligible. Comparable values were found for all other conditions and subjects.

Except for the smallest relative damping β at the smallest eigenfrequency f_{0_i}, high VAF values ($> 83\%$) were obtained (Fig. 8, bottom row), which can be considered very good. This means that the linear model structure with the estimated parameter values $\hat{k}_p$, $\hat{k}_v$ and $\hat{u}_0$, is an accurate approximation of the real system dynamics (arm plus environment) under these experimental conditions.

Figure 9 shows the difference between the scaled RMS of the EMG signals and corresponding estimated cocontraction levels $\hat{u}_0$. Since the RMS values were scaled such that their means coincide with the estimations, the mean of the difference is zero. For each muscle, the standard deviations amongst all subjects are indicated by dotted lines. The EMG of the deltoideus anterior showed the largest differences (24% SD) while the discrepancies of the other muscles were smaller ($\leq 18\%$). For subjects H.V. and J.V. the differences were small for deltoideus anterior, meaning that the variations of the estimated cocontraction levels approximated those of the EMG recordings very well. The same accounts for the pectoralis major (subjects H.B. and H.V.) and deltoideus posterior (subject H.B.). The mean standard deviation of all muscles and subjects was $\approx 20\%$. The effect of these variations in cocontraction level on the estimated feedback gains is analysed by optimizations and described at the end of Sect. 3.2.

3.2 Optimization

Metabolic energy weighting was not incorporated in our model, so that unrealistic high values of intrinsic stiffness and damping resulted when the amount of cocontraction was taken as a free parameter to be optimized. Therefore, its value (i.e. u_0) was fixed to the corresponding estimated value for each condition.

Figure 10 shows the averaged estimated length and velocity feedback gains together with the optimized values for a number of different values of control-effort weighting factor p. Both optimized reflex gains for outranged the estimated values ($k_p^* > 8000$ N/m, $k_v^* > 500$ N/m) for $p = 0$ (not shown). The optimized gains decreased with increasing control-effort weighting. Negative values for k_v^* were also not found for very large p values. All values of the estimated length feedback gains are within the range of the optimized values for different p. The predicted velocity feedback gains were substantially lower in all cases. This indicates that the estimated reflexive velocity feedback is suboptimal under these experimental conditions.

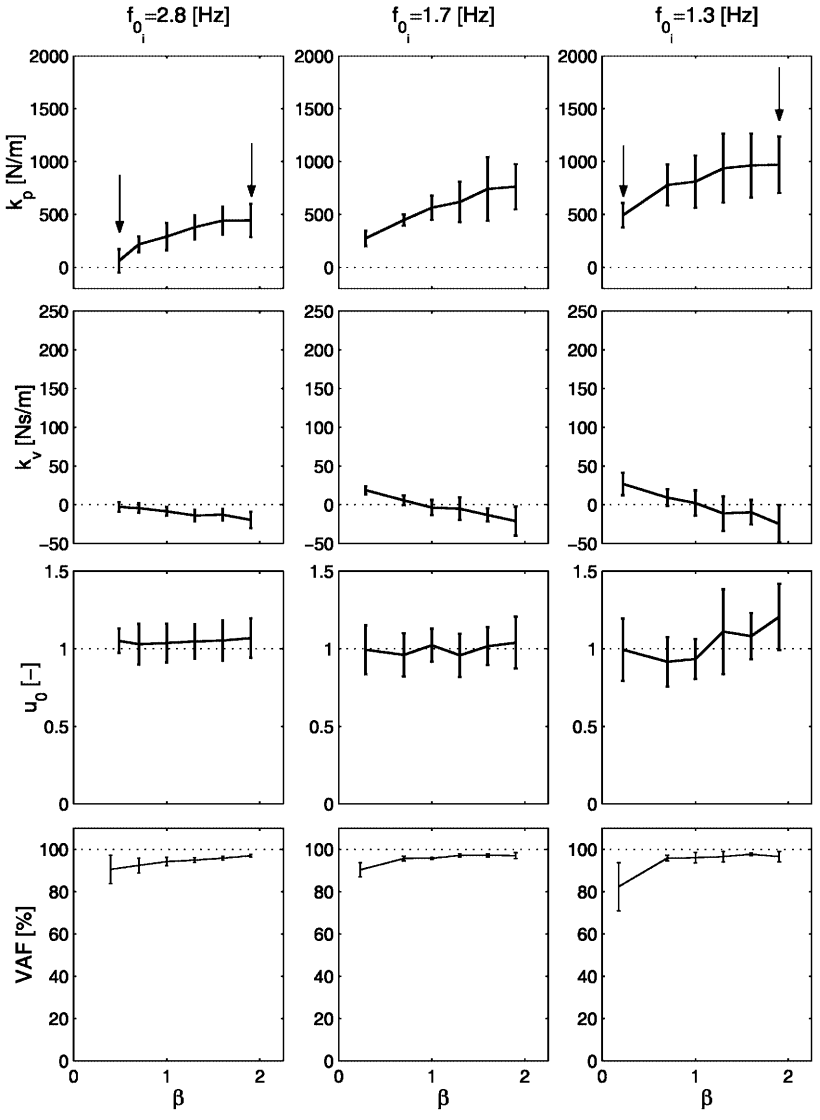

Fig. 8. Estimated mean reflex gains and standard deviation (*error bars*) averaged over all subjects ($n = 5$). *Rows* from *top* to *bottom*: length feedback gain $\hat{k}_{\mathrm{p}}$, velocity feedback gain $\hat{k}_{\mathrm{v}}$, cocontraction level $\hat{u}_0$ and variance accounted for (VAF) values. *Columns*: *left*, $f_{0_{\mathrm{i}}} = 2.8$ Hz; *middle*, $f_{0_{\mathrm{i}}} = 1.7$; *right* $f_{0_{\mathrm{i}}} = 1.3$ Hz. *Vertical arrows* indicate the conditions for which the frequency response functions (FRFs) of the combined system and the arm are shown in Figs. 6 and 7 (i.e. the large circles in Fig. 5)

To show the role of velocity feedback, Fig. 11 displays the optimized length feedback gains again for the same p values but without velocity feedback; i.e. k_{v}^* was set to zero as an approximation of the estimated values. The curvatures of k_{p}^* are similar, except in case of the lowest relative damping β at the two largest eigenfrequencies $f_{0_{\mathrm{i}}}$.

The impact of control-effort weighting on performance and afferent feedback is shown in Fig. 12 for three values of β (0.7, 1.3, and 1.9) at each eigenfrequency. As expected, the performance worsens with control-effort weighting for all conditions, as can be seen by the increase of the performance criterion function J_x (Fig. 12, top row). For the highest eigenfrequency, the performance without control-effort weighting ($p = 0$) was the worst and therefore the relative increase of J_x was smallest. Control effort is effectively reduced for small weightings and saturated when weighting was further increased (Fig. 12, middle row). Slightly weighting J_a with p also improved converging of the parameters significantly. The contribution of J_x to J is much higher than that of pJ_a, as can be seen by comparing J_x and J (Fig. 12, bottom row and top row).

One value for control-effort weighting was chosen for all conditions, $p = 0.5 \times 10^{-7}$, as indicated by the grey vertical lines in Fig. 12. With this value the control effort J_a was substantially reduced (≈60–80%), while performance J_x decreased to a far lesser extent ($\leq 20\%$, see Fig. 12). The corresponding optimized length reflex gains k_{p}^* are shown in Fig. 13 (k_{v}^* set to zero). Apart from the two largest eigenfrequencies and smallest relative damping, the gains were predicted quite well and captured by the standard deviations of the corresponding estimates.

Figure 14 shows the effect of variations in cocontraction level on the reflex gains ($p = 0.5 \times 10^{-7}$). When estimated cocontraction levels were increased by 20% (i.e. a proportional increase of muscle stiffness and damping), both the reflex gains decreased only slightly ($\leq 10\%$) for all conditions, and vice versa in case of lower cocontraction.

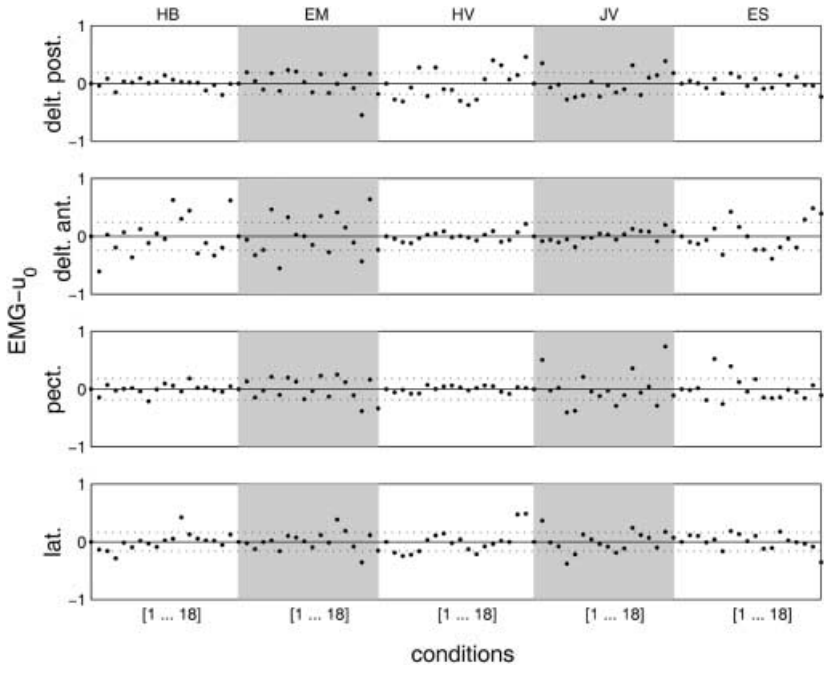

Fig. 9. Difference of measured EMG (scaled RMS) and estimated cocontraction $\hat{u}_0$ indicated by points for all of the MB combinations for each muscle (*rows*) and all subjects (*white–grey columns*) with standard deviations (*horizontal dotted lines*). Each *column* shows all eighteen MB combinations per subject

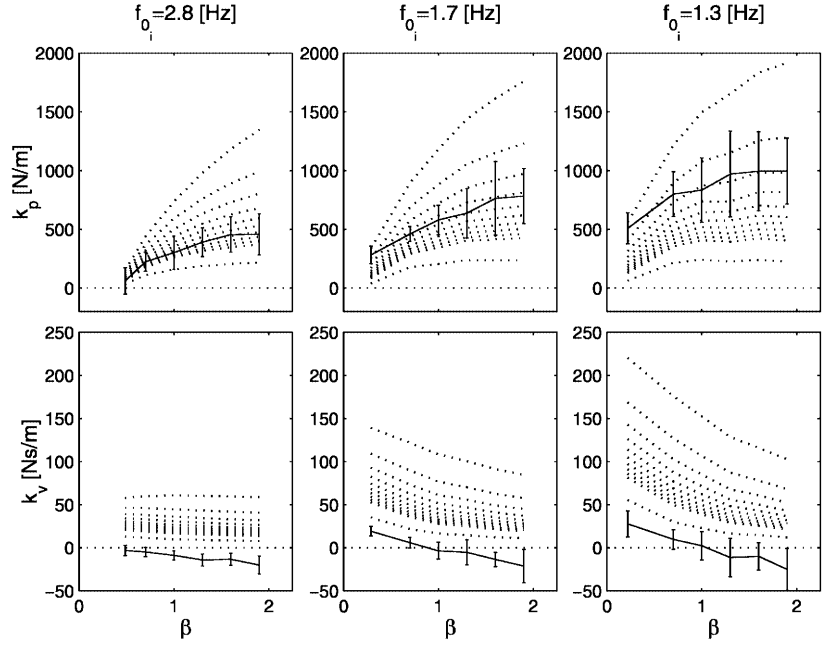

Fig. 10. Optimized (*dashed curves*) and estimated (*solid curves*) reflex gains, averaged over all subjects ($n = 5$). *Error bars* denote the standard deviation of the estimated mean values. Each *dotted line* corresponds to one value of p in the range $\{0.1-2.0\} \times 10^{-7}$. The largest optimized gains occurred at the lowest values of p

4 Discussion

The stability of the combined system was guaranteed for all conditions. Apart from the smallest relative damping at each eigenfrequency, the combined system was sufficiently damped (Fig. 7). This is because the external dynamics provided substantial damping. Consequently, the human controller was indemnified from critically controlling the stability margins of the total system by being only partly able to change the admittance of the combined system. The adjustments of reflexive feedback gains under those current experimental conditions were therefore particularly determined by performance and control-effort criteria and not constrained by stability demands, as was the case in previous studies (De Vlugt et al. 2001; Schouten et al. 2001).

To clarify the changes in reflex gains, it must be repeated that performance J_x is related to the combined system of arm plus environment (Eq. 12), and the only way to improve performance is to modify the arm admittance. To what extent the performance is determined by the arm also depended on the mechanical properties of the environment. Because only the damping and the mass of the environment were increased, the stiffness was always determined by the arm only, i.e. by intrinsic and reflexive feedback. This is the reason

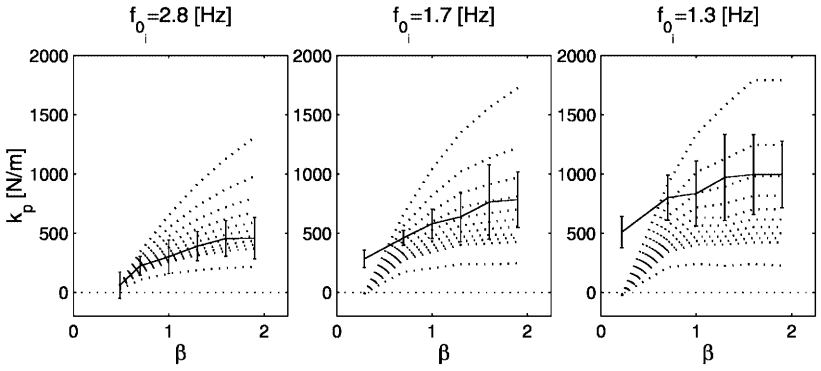

Fig. 11. Optimized (*dashed curves*) and estimated (*solid curves*) length reflex gain; averaged over all subjects ($n = 5$). Velocity feedback is not optimized, and is set to zero. *Error bars* denote the standard deviation of the estimated mean values. Each *dotted line* corresponds to one value of p in the range $\{0.1-2.0\} \times 10^{-7}$. The largest optimized gains occurred at the lowest values of p

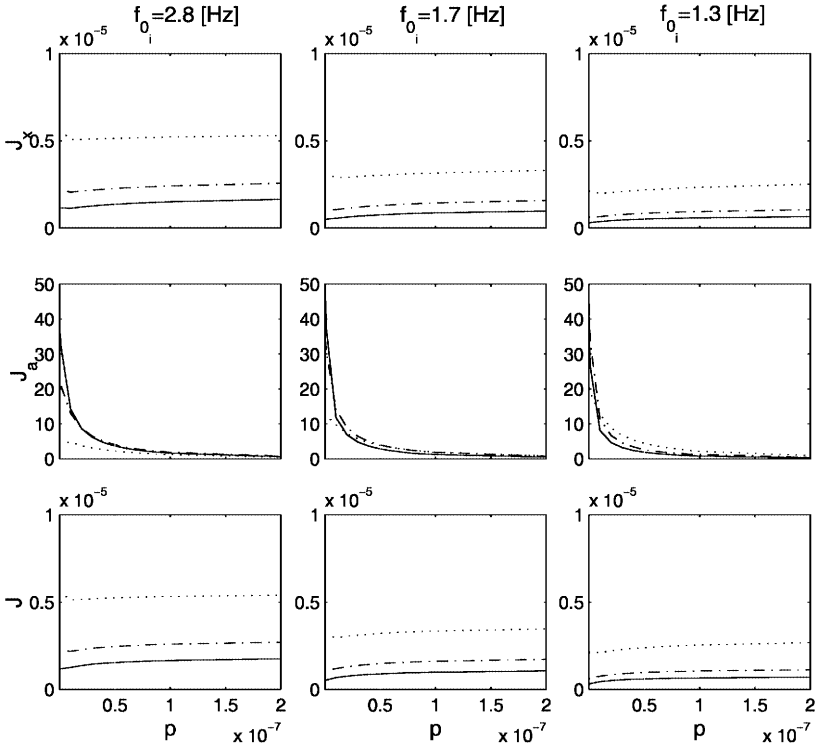

Fig. 12. Criterion functions for different values of control-effort weighting p. *Top row*: performance criterion J_x; *middle row*: control-effort criterion J_a; *bottom row*: summed criterion J. *Dotted curves*: $\beta = 0.7$; *Dashed–dotted curves*: $\beta = 1.3$; *Solid curves*: $\beta = 1.9$. Criterion values at $p = 0.5 \times 10^{-7}$ are indicated by grey *vertical lines*

why increasing arm stiffness by high length feedback gains was effective in general for nearly all experimental conditions.

In the case of the highest eigenfrequency f_{0_i} and the smallest relative damping β (minimal mass and damping of the environment), the combined system was dominated by the mechanical properties of the arm. For this condition, both reflex gains were found to be very small (Fig. 10), as was also found in a comparable study by Van der Helm (submitted, 2002) and in previous simulation studies (De Vlugt et al. 2001; Schouten et al. 2001). The absence of reflexes for this condition can be explained from the effect of k_p on J_x, which is twofold. First, as already stated above, it increases stiffness which is beneficial. Second, it directly decreases relative damping, according to (8) and due to the neural time delay. Obviously, smaller relative damping increases the amplification at system's eigenfrequency (oscillation) that deteriorates performance. Apparently, a negative contribution of an oscillation peak is larger than a profitable increase of stiffness for this condition. The absence of feedback also validated the estimation of the intrinsic parameters which were estimated in this condition.

When relative damping increases, the influence of an increased oscillation peak of the arm dynamics has little effect on the combined system and consequently worsens performance to a lesser extent. This is simply because the overall damping is larger. Therefore, k_p can be increased to improve performance in these cases. Generally, the higher the total relative damping the larger the efficiency of length feedback because amplification at the eigenfrequency of the arm is suppressed by the environment.

The velocity feedback gain $\hat{k}_v$ was very small, decreased slightly and even became negative for larger relative damping. [Note that negative reflex gains were also found by Van der Helm (submitted, 2002), were close to optimal under the experimental conditions (De

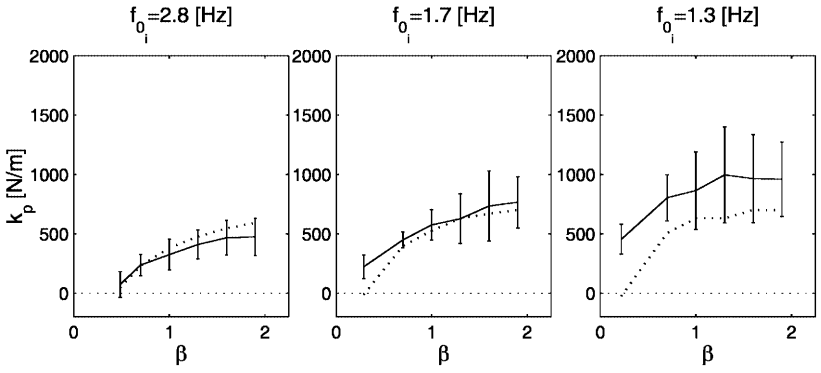

Fig. 13. Optimized (*dashed curves*) and estimated (*solid curves*) length feedback gains, averaged over all subjects ($n = 5$). Velocity feedback is not optimized, and is set to zero. Control-effort weighting $p = 0.5 \times 10^{-7}$. *Error bars* denote the standard deviation of the estimated mean values

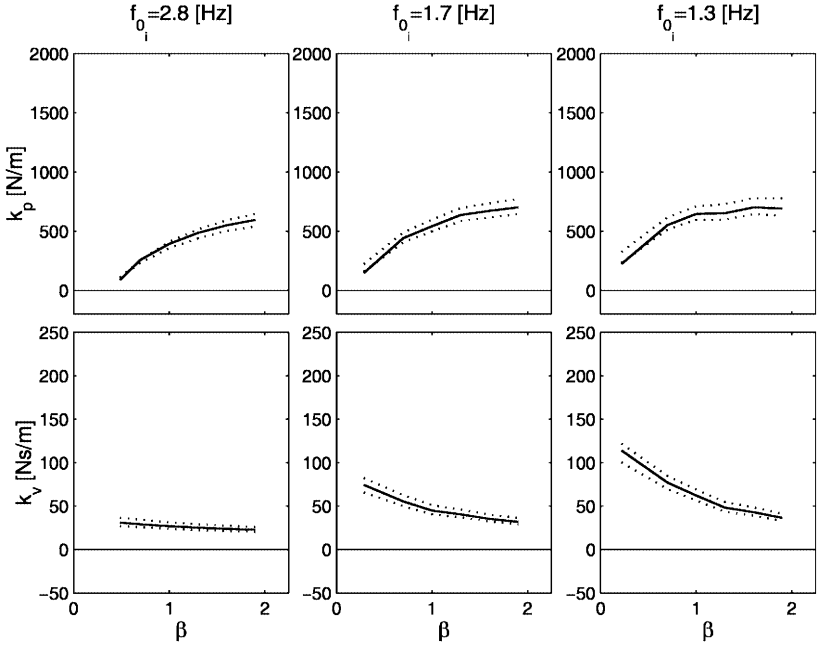

Fig. 14. Model optimization ($p = 0.5 \times 10^{-7}$) showing the effect of variations in cocontraction level on the reflex gains. *Solid curves*: optimized gains using the corresponding estimated values for u_0. *Dotted curves*: u_0 is increased (*below*) and decreased (*above*) with 20%

Vlugt et al. 2001) and were attributed to autogenic excitation (A. C. Schouten, submitted, 2002)]. On the contrary, the simulation results showed k_v^* was substantial and effectively suppressed the resonance peak in particular for the smallest eigenfrequency and smallest relative damping. This is shown in Fig. 15 (right upper plot, dashed-dotted curves). The estimated $\hat{k}_v$ therefore seems suboptimal and leaves the arm and combined system underdamped, in particular for this condition (Fig. 15, right upper plot, solid curves). When velocity feedback gain was fixed to zero, the lack of damping is evidently predicted but now the optimized length feedback gains were much smaller than estimated for these particular conditions, resulting in an increase of the low-frequency gain of $H_{DX}(f)$ (Fig. 15, right upper plot, dotted curves). Apart from this extreme condition, the length feedback appears to be close to optimal and the estimated FRFs of the combined system $H_{DX}(f)$ were very similar to the optimized ones.

It is possible that the length and velocity feedback gains are somehow restricted by a mutual gain-limiting relation which was not incorporated in our model (Schaafsma et al. 1991). For instance, if muscle spindle output was dependent on the amplitude of velocity such that at large velocities the sensitivity for lengthening was reduced and vice versa, at low velocities length feedback would be more dominant. Apparently, if such mechanisms somehow exist, the movements in our experiments were slow enough to exhibit pronounced length feedback in nearly all cases. Omitting the velocity feedback from the optimization was a means to mimic such a property. Further research on spindle transfer-function identification is necessary to explain such input selectivity and to clarify the restricted velocity gains found under the current experimental conditions.

Summarizing the findings it is stated that (1) length feedback effectively reduces the admittance of the combined system and (2) the strength of length feedback is the result of weighting of admittance reduction against the control effort needed for this reduction.

We have also applied slower time constants (30–50 ms) for the activation process and found that the estimated velocity feedback gains increased while length feedback did not noticeably change (not shown). This is because activation acts as a low-pass filter ($\approx$5 Hz) to

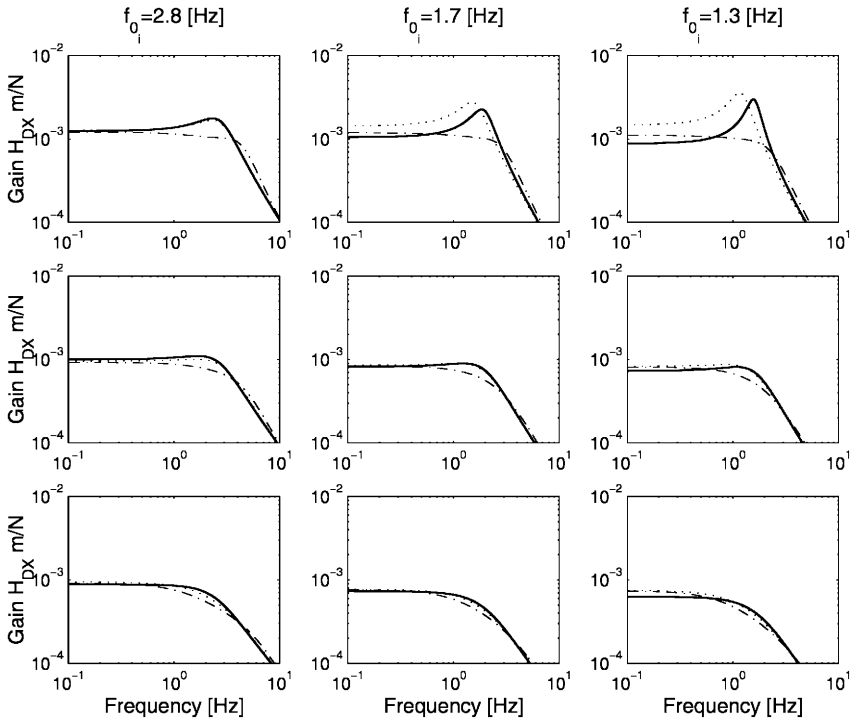

Fig. 15. FRFs of modelled combined system $H_{DX}(f)$ for smallest relative damping β (*top row*), $\beta = 1.0$ (*middle row*) and $\beta = 1.6$ (*bottom row*) at all three eigenfrequencies f_{0_i}. *Solid curves* are the combined model parametrized with the estimated parameters $\hat{k}_p$, $\hat{k}_v$ and $\hat{u}_0$ (mean of all subjects). *Dashed–dotted curves*: the optimized FRFs parametrized with optimal gains k_p^* and k_v^* for $p = 0.5 \times 10^{-7}$. *Dotted curves*: the optimized FRFs parametrized with the optimal gain k_p^* and k_v^* set to zero for the same weighting factor

afferent signals such that higher velocity gains would be estimated to obtain the same behaviour. This sensitivity of velocity feedback on activation time constant can account for the unexpected negative values. However the same sensitivity also follows from the model optimization and so the discrepancy with the estimated velocity gains still remains.

Mean EMG and estimated cocontraction levels were almost constant over the conditions. Since increasing intrinsic stiffness and damping always improves performance, cocontraction was apparently at maximum during all conditions. The difference between recorded EMG and estimated cocontraction level had a standard deviation of $\approx 20\%$, accounting for measurements noise and inaccuracy of the estimation procedure. Higher cocontraction levels decreased the admittance of the combined system due to larger intrinsic stiffness and damping of the arm. Consequently, at the same weighting of control effort, the effectiveness of additional reflexive feedback was less and the gains were smaller (Fig. 14). The opposite effect was shown for smaller cocontraction levels. However, the effect of fluctuations in cocontraction did not affect the values of the feedback gains substantially and therefore do not change the findings of this study. A 20% variation merely changed the gains by less than 10%. This indicated the estimation procedure was accurate enough to quantify intrinsic and reflexive properties, which was confirmed by high VAF values.

Subjects felt that they had the least control over the combined system at the lowest eigenfrequencies f_{0_i}. In these cases, both the mass and the damping of the environment were large. This was reflected by increased variations in cocontraction ($\hat{u}_0$ and EMG) and larger standard deviations in estimated length reflex gains (Fig. 8). This varying behaviour is most likely the result of decreased relative contribution of the arm damping to the damping of the combined system, so that subjects possibly varied slightly around their optimal adjustments without affecting performance seriously.

Despite the rather good resemblance of estimated cocontraction level and measured EMG, it must be mentioned that EMG is not a direct measure for muscle force. Since (non-linear) activation dynamics separate these quantities a direct comparison seems impossible. However, in a mean sense for almost constant cocontraction levels, the activation dynamics can be neglected such that muscle force can be taken as a scaled version of the corresponding EMG. Since EMG and u_0 were both used as normalized variables in this study, a direct comparison was justified.

5 Implications

Despite the highly non-linear nature of the neuromuscular system, the mechanical behaviour was well described by a linear model for all experimental conditions applied. At the muscle level, most relevant non-linearities are the unidirectional (stretch amplitude and velocity) sensitivity of the spindles (e.g. Stein and Kearney 1995), different calcium activation–deactivation rates, and mechanical properties such as the force–length and force–velocity characteristics. In multiple muscle systems these non-linearities apparently cancel out at the end point level under specific conditions. The linear behaviour demonstrated in the case of this study can be explained by the following arguments: (1) the application of small-amplitude disturbances does not excite non-linearities; (2) unidirectionality in sensor sensitivity and muscle force generation presumably turns

into bi-directional behaviour in the case of muscles acting as antagonistic pairs; and (3) from a functional anatomical point of view, different muscles are likely to act at different lengths and hence distribute their characteristics over a wider range of motion which smooths out the non-linearities. Furthermore, non-linearities from inertial properties (configurational, centripetal, and Coriolis) can be considered negligible for the perturbations used because the angular excursions were small.

The application of a linear model is further supported by a phenomenon found by Kirsch et al. (1994). They demonstrated that stochastic perturbations tends to linearize the intrinsic muscle response, probably because of changed dynamics of the cross-bridge turn over. In particular, stiffness properties were found to remain constant and not exhibit a dependence on displacement amplitude, even for movements which significantly exceeded the yield length revealed by step stretches.

The interaction of the human arm with an environment and the adjustments of intrinsic and reflexive properties were considered optimal for the specific task. The experimental conditions represented a variety of different environmental admittances. The results clearly demonstrated that reflexes were adapted such that the task 'minimize displacements' during continuous force perturbation was indeed performed near optimally by the subjects. The high VAF values indicate that the model is an adequate description of the mechanical response of the arm at the end point level. The modulation of the reflex gains, in particular that of muscle length, seemed to follow a precise weighting of stiffness enlargement against a smaller relative damping. And such gain modulations obviously took place within seconds. The short latency of 25 ms suggests that the reflexive contribution was from monosynaptic pathways. It is possible that these adaptations are accomplished by specific controlled presynaptic depolarization of afferent terminals that reduces feedback sensitivity of the motoneuron (Rudomin 1999).

The results from this study correspond to those of Milner and Cloutier (1993), who found experimental evidence that monosynaptic reflexes are adapted to different external dynamics. Their results are comparable in the sense that they found the same effects in the opposite direction, namely that feedback gain decreased with increasing (positive) velocity feedback of the manipulator. The results from this study support these findings in a more specific way, by showing that humans act like optimal controllers to optimize the combined dynamics of limb and environment together. Under the current experimental conditions (i.e. continuous unpredictable force perturbation while maintaining a reference position) short-latency reflex gain adjustment appear to be quite effective in performing such optimizations.

These results are in contrast to others suggesting that any gain adaptation may not be a usual mechanism by which the stretch reflex is controlled (Crago et al. 1976; Jaeger et al. 1982; Lee and Tatton 1975). From those studies the effect of different tasks on reflex action of the human elbow muscles was investigated and considerable changes in the short latency stretch reflex were not found. However, they neither changed the properties of the force perturbation nor varied the external dynamics to assess reflex gain adjustment. Just like the majority of studies aiming to reveal the function of reflexive feedback, these researchers applied transient perturbations that did not allow sufficient time for the human controller to adapt to the mechanical environment, let alone to optimize some sort of a performance measure in the presence of perturbations (Carter et al. 1993; Houk 1978; Stein and Kearney 1995; Toft et al. 1991). In fact, those experiments aim to measure the state of the subject at the time just before onset of the perturbation rather than the performance of the reaction. In accordance with Smeets and Erkelens (1991), we believe that transient-like perturbations are somewhat poor test signals for eliciting short-latency gain modulation. Because short latency length reflexes varied substantially during our experiments, continuous random force perturbations have been proved better suited to investigate reflex control (Agarwal and Gottlieb 1977b; Dufresne et al. 1978).

Control-effort weighting had a great impact on the reflex gains. This simply meant that when performance improvement was small with a modest increase of feedback gains, control-effort weighting highly suppressed reflexive activation. The results from the model optimization suggests that humans optimize performance with limited afferent control effort. Since zero weighting would result in the best performance (but excessively high gains), the weighting factors found were probably as small as possible. It is unclear which mechanisms contribute to the weighting or limitation of afferent control effort, and a single parameter is likely too simple to describe the underlying mechanism. However, the predicted length reflex gains showed strong resemblance with the estimated gains when the velocity feedback was omitted from the optimization. These results indicate the presence of some kind of restricting mechanism between afferent static and dynamic information.

Agarwal and Gottlieb (1977a) perturbed the ankle joint with a random 0–50 Hz force perturbation while the subjects were instructed to counteract various bias torques such that foot movement was symmetrical with respect to a reference angle. The mechanical environment was formed only by the inertia of the footplate, which was slightly larger than that of the foot. They did not find a distinct resonance peak, and their corresponding FRF of the ankle admittance was quite similar with the responses from this study where reflexive feedback was absent (Fig. 7, left column, dotted curve). At least the argument of Agarwal and Gottlieb (1997a) that reflexive feedback were not functional during random perturbations per se is strongly contradicted by the results of this study. Their conclusion is misleading and can be attributed to the fact that both task instruction and perturbation were force based. This results in unnatural adjustments of the limb, i.e. the only way to maintain a mean force level while the limb is being

perturbed is to move in the same directions as the force perturbation, which for random signals is impossible. Therefore, the limb stiffness had to be kept small so as to approximate such (unnatural) behaviour. Most likely, reflexive gain control during force perturbations is not suited to force tasks but is highly suited to position tasks.

6 Conclusions

Afferent length and velocity feedback gains were shown to adapt to different mechanical properties of the environment. In particular, length feedback gain increased substantially with relative damping of the combined system. Increasing the eigenfrequency by using larger masses of the environment increased the length feedback gains to a lesser extent. These modulations of gains served the optimization of a performance criterion concerning the combined system of arm plus environment, i.e. the minimization of displacements of the hand during a continuous force perturbation. It is likely that the CNS controls the reflex gains within seconds after the perturbation was applied. This specialized feedback behaviour followed directly from optimal control theory. Length feedback effectively improved performance because it enlarges stiffness, but only when its negative side effect of increased resonance is suppressed by the environment.

Model optimizations show strong similarities with the estimated length feedback gains indicating that: (1) the performance criterion is a realistic description of the task instruction; (2) the control-effort weighting is somehow apparent in the feedback loop; and (3) because of the high VAF values, the model is an adequate description of intrinsic and reflex mechanisms at the end point level.

The results are valid for the system being perturbed with continuous random forces while the subject is performing a position task. Because these conditions correspond to real-life posture maintenance, it is believed that these conditions are necessary to explain neuromuscular functioning of human posture control in vivo.

Appendix A: Model development comprising dynamics of arm, hand and environment

In this study only the end point dynamics are identified, representing the lumped effect of joint dynamics at hand level. It consists of four parts: (1) the intrinsic arm mass, damping and stiffness; (2) the (intrinsic) hand damping and stiffness; (3) the reflexive length and velocity feedback including muscle activation; and (4), the external mass, damping and stiffness of the environment. Figure A1 shows the compound block diagram of all different parts.

The model is expressed in the frequency domain where the higher derivatives are given as powers of the Laplace operator $s\,(=\lambda+j2\pi f)$.

A.1 Intrinsic part

For small displacements the viscoelastic properties of muscles can be described well by a linear spring–damper system. Together with the arm mass the intrinsic properties are modelled as

$$H_{\mathrm{i}}(s)=\frac{X_{\mathrm{a}}(s)}{F_{\mathrm{int}}(s)}=\frac{1}{m_{\mathrm{a}}s^2+(b_{\mathrm{a}}s+k_{\mathrm{a}})u_0} \tag{A1}$$

Any stiffness and viscosity from passive tissues surrounding muscles and joints are also included in the model. The amount of cocontraction is represented by u_0 and scales intrinsic stiffness and damping, which seems to be justified (Agarwal and Gottlieb 1977a). In the case of silent reflexes, i.e. when the intrinsic model is estimated, u_0 is set to one as a reference.

The spring–damper system k_{h} and b_{h} acts in series with the arm dynamics, representing the interaction of the hand with the handle. The position of the handle x_{h} in the model is different from the position of the arm x_{a} (Fig. A1) and represents movement of the wrist, skin displacement and movement of the fingers:

$$H_{\mathrm{h}}(s)=\frac{F_{\mathrm{h}}(s)}{X_{\mathrm{h}}(s)-X_{\mathrm{a}}(s)}=b_{\mathrm{h}}s+k_{\mathrm{h}} \tag{A2}$$

The intrinsic arm model becomes $[F_{\mathrm{int}}(s)=F_{\mathrm{h}}(s)]$

$$\frac{X_{\mathrm{h}}(s)}{F_{\mathrm{h}}(s)}=\frac{1+H_{\mathrm{h}}(s)H_{\mathrm{i}}(s)}{H_{\mathrm{h}}(s)}=H_{\mathrm{h}}^{-1}(s)+H_{\mathrm{i}}(s) \tag{A3}$$

The intrinsic parameters to be estimated are m_{a}, b_{a}, k_{a}, b_{h} and k_{h} ($u_0=1$).

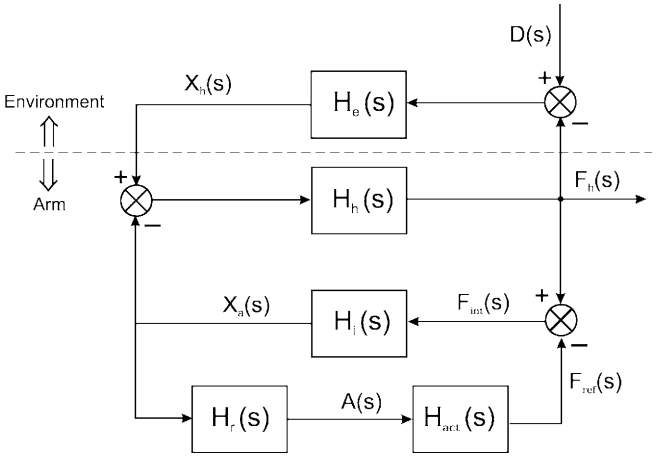

Fig. A1. Block diagram of the combined arm–hand–environment model expressed in the frequency domain. Arm dynamics (indicated below the *dashed border line*) consist of H_{r}, reflexive length and velocity feedback; H_{act}, activation dynamics; H_{i}, intrinsic arm dynamics; and H_{h}, hand dynamics. H_{e} represents the dynamics of the environment (above the *dashed line*). $X_{\mathrm{a}}(s)$ is the position of the arm, $X_{\mathrm{h}}(s)$ the (measured) position of the hand, $F_{\mathrm{h}}(s)$ the (measured) interaction force applied by the hand, $F_{\mathrm{int}}(s)$ the intrinsic force, $F_{\mathrm{ref}}(s)$ the reflexive force, $A(s)$ is the reflexive activation, and $D(s)$ is the applied external force perturbation

A.2 Reflexive part

Spindle dynamics are described by a first-order transfer function $H_r(s)$, relating arm position $X_a(s)$ to the afferent neural signal $A(s)$ (Fig. A1) according to

$$H_r(s) = \frac{A(s)}{X_a(s)} = (k_v s + k_p)e^{-T_d s} \tag{A4}$$

Linear approximation of the spindle dynamics seems to be justified during the small stationary periodic perturbations as used in this study (Soechting and Dufresne 1980; Zahalak and Pramod 1985). The reflex gains k_p and k_v represent the reflexive position and velocity feedback gains, respectively. Transmission delay and processing time in the spinal cord are described by a time delay $T_d = 25$ ms (Smeets and Erkelens 1991).

Activation and deactivation processes of the muscle are approximated by a first-order system with a time constant $\tau_a = 30$ ms (Winters and Stark 1985):

$$H_{act}(s) = \frac{F_{ref}(s)}{A(s)} = \frac{1}{\tau_a s + 1} \tag{A5}$$

Intrinsic arm (without hand dynamics) and reflexive feedback can now be formulated as

$$H_a(s) = \frac{X_a(s)}{F_h(s)} = \frac{H_i(s)}{1 + H_i(s)H_r(s)H_{act}(s)} \tag{A6}$$

which forms the feedback path to the hand dynamics $H_h(s)$, resulting in the arm dynamics (including the hand) $H_{arm}(s)$:

$$H_{arm}(s) = \frac{X_h(s)}{F_h(s)} = H_h^{-1}(s) + H_a(s) \tag{A7}$$

A.3 Combined model: arm plus environment

The environment acts in parallel with the arm and hand, where the sum of the reaction force at the hand and the external force perturbation forms the input (Fig. A1). The second-order dynamics of the environment equals

$$H_e(s) = \frac{X_h(s)}{D(s) - F_h(s)} = \frac{1}{m_e s^2 + b_e s + k_e} \tag{A8}$$

where m_e is the mass, b_e is the viscosity and k_e the stiffness of the environment. The complete model including the environment becomes

$$H_{DX}(s) = \frac{X_h(s)}{D(s)} = \frac{H_e(s)}{1 + H_e(s)H_{arm}^{-1}(s)} \tag{A9}$$

As part of the optimization, $H_{DX}(s)$ is used for calculating the cost function J_x and the poles for assessing the system's stability.

For calculating the control-effort cost function J_a, the closed-loop function $H_{DA}(s)$ is used. Therefore, the afferent reflexive signal $A(s)$ (Fig. A1) is first expressed as

$$A(s) = H_r(s)X_a(s) \tag{A10}$$

Substituting (A6), (A7) and (A9) in (A10) gives

$$H_{DA}(s) = \frac{A(s)}{D(s)} = H_r(s)H_a(s)H_{arm}(s)H_{DX}(s) \tag{A11}$$

A.4 Frequency domain form of J_x

The task instruction '*minimize the displacements*' is represented mathematically in the form of a cost function to be minimized. Having a linear, noise-free system with stationary stochastic inputs, the cost function J of the displacement $x(t)$ is

$$J_x = E\{x^2(t)\}$$

where $E\{\cdot\}$ is the expectation operator. When $E\{x(t)\} = 0$, J_x is the variance σ_x^2 of $x(t)$. By using the following relations:

$$J_x = \sigma_x^2 = \int_{-\infty}^{\infty} S_{xx}(f)\mathrm{d}f = 2 \cdot \int_{0^+}^{\infty} S_{xx}(f)\mathrm{d}f$$

and

$$S_{xx}(f) = E\{X(f) \cdot X(-f)\}$$
$$X(f) = H_{DX}(f) \cdot D(f)$$

J_x can be rewritten in the frequency domain:

$$J_x = 2 \cdot \int_{0^+}^{\infty} |H_{DX}(f)|^2 S_{dd}(f)\mathrm{d}f$$

$S_{dd}(f)$ is the power spectrum of the input signal. The system inputs have rectangular power spectra:

$$S_{dd}(f) = c \quad \forall f_l \le f \le f_h$$

and zero elsewhere, so that J_x can be written as

$$J_x = c \cdot \int_{f_l}^{f_h} |H_{DX}(f)|^2 \mathrm{d}f \tag{A12}$$

where c is set to one.

References

Agarwal GC, Gottlieb CL (1977a) Compliance of the human ankle joint. J Biomech Eng 99: 166–170

Agarwal GC, Gottlieb CL (1977b) Oscillation of the human ankle joint in response to applied sinusoidal torque on the foot. J Physiol (Lond) 268: 151–176

Bennett DJ, Gorassini M, Prochazka A (1993) Catching a ball: contributions of intrinsic muscle stiffness, reflexes, and higher order responses. Can J Physiol Pharmacol 72: 525–534

Carter RR, Crago PE, Gorman PH (1993) Nonlinear stretch reflex interaction during cocontraction. J Neurophysiol 69: 943–952

Crago PE, Houk JC, Hasan Z (1976) Regulatory actions of human stretch reflex. J Neurophysiol 39: 925–935

De Vlugt E, Van der Helm FCT, Schouten AC, Brouwn GG (2001) Analyses of the reflexive feedback control loop during posture maintenance. Biol Cybern 84: 133–141

Doemges F, Rack PMH (1992a) Changes in the stretch reflex of the human first dorsal interosseous muscle during different tasks. J Physiol (Lond) 447: 563–573

Doemges F, Rack PMH (1992b) Task-dependent changes in the response of human wrist joints to mechanical disturbance. J Physiol (Lond) 447: 575–585

Dufresne JR, Soechting JF, Terzuolo CA (1978) Electromyographic response to pseudo-random torque disturbances of human forearm position. Neuroscience 3: 1213–1226

Hogan N (1985) The mechanics of multi-joint posture and movement control. Biol Cybern 52: 315–331

Houk JC (1978) Participation of reflex mechanisms and reaction-time processes in the compensatory adjustments to mechanical disturbances. In: Desmedt JE (ed) Cerebral motor control in man: Long Loop Mechanisms. Prog Clin Neurophysiol 4. S. Karger, Basel: 193–215

Jaeger RJ, Gottlieb GL, Agarwal GC (1982) Myoelectric responses at flexors and extensors of human wrist to step torque perturbations. J Neurophysiol 48: 388–402

Jenkins GM, Watts DG (1969) Spectral analysis and its applications. Holden Day, San Francisco

Kirsch FK, Boskov D, Rymer WZ (1994) Muscle stiffness during transient and continuous movements of cat muscle: perturbation characteristics and physiological relevance. IEEE Trans Biomed Eng 41: 758–770

Lacquaniti F, Soechting JF (1986) Simulation studies on the control of posture and movement in a multi-jointed limb. Biol Cybern 54: 367–378

Lee RG, Tatton WG (1975) Motor responses to sudden limb displacements in primates with specific CNS lesions and in human patients with motor system disorders. Can J Neurol Sci 2: 285–293

Milner TE, Cloutier C (1993) Compensation for mechanically unstable loading in voluntary wrist movement. Exp Brain Res 94: 522–532

Rudomin P (1999) Presynaptic selection of afferent inflow in the spinal cord. J Physiol (Paris) 93: 329–347

Schaafsma A, Otten E, Van Willigen JD (1991) A muscle spindle model for primary afferent firing based on a simulation of intrafusal mechanical events. J Neurophysiol 65: 1297–1312

Schouten AC, De Vlugt E, Van der Helm FCT, Brouwn GG (2001) Optimal posture control of a musculo-skeletal arm model. Biol Cybern 84: 143–152

Smeets JB, Erkelens CJ (1991) Dependence of autogenic and heterogenic stretch reflexes on pre-load activity in the human arm. J Physiol (Lond) 440: 455–465

Soechting JF, Dufresne JR (1980) An evaluation of nonlinearities in the motor output response to applied torque perturbations in man. Biol Cybern 36: 63–71

Stein RB, Kearney RE (1995) Nonlinear behavior of muscle reflexes at the human ankle joint. J Neurophysiol 73: 65–72

Toft E, Sinkjær T, Andreassen S, Larsen K (1991) Mechanical and electromyographic responses to stretch of the human ankle extensors. J Neurophysiol 65: 1402–1410

Van Lunteren T (1979) Identification of human operator describing function models with one or two inputs in closed loop systems. PhD thesis, Delft University of Technology, The Netherlands

Winters JM, Stark L (1985) Analysis of fundamental human movement patterns through the use of in-depth antagonistic muscle models. IEEE Trans Biomed Eng 32: 826–839

Zahalak GI, Pramod R (1985) Myoelectric response of the human triceps brachii to displacement-controlled oscillations of the forearm. Exp Brain Res 58: 305–317